nature portfolio

https://doi.org/10.1038/s41589-021-00740-7

Supplementary information

Optical control of fast and processive engineered myosins in vitro and in living cells

In the format provided by the authors and unedited

Supplementary Material

Optical control of fast and processive engineered myosins *in vitro* and in living cells

Paul V. Ruijgrok, Rajarshi P. Ghosh, Sasha Zemsky, Muneaki Nakamura, Rui Gong, Lin Ning, Robert Chen, Vipul T. Vachharajani, Alexander E. Chu, Namrata Anand, Raphael R. Eguchi, Po-Ssu Huang, Michael Z. Lin, Gregory M. Alushin, Jan T. Liphardt, and Zev Bryant

Supplementary notes

Supplementary Note 1. Modeling gliding velocity as function of light dose

We discuss a simple model to describe the light dose dependent response of a gliding filament assay with optically active motors. Our approach follows the framework of Vilfan[1], which builds on the 'rower' model by Leibler and Huse[2] and neglects effects such as strain dependence of transition rates, reverse transitions, and non-linearities in the elasticity.

Following Vilfan, we describe the gliding motility assay by considering an actin filament interacting with an ensemble of motors, giving a force balance equation

$$F = \langle N \rangle \kappa \left(\langle \xi \rangle - \langle X \rangle \right) \qquad \textit{Eq. 1}$$

where N is the number of motors bound to the filament and κ is the spring constant of a single motor crosslink. Each crosslink is stretched by a displacement ξ due to the stroke vector, modified by an accumulated displacement X during filament gliding. The angle brackets $\langle \dots \rangle$ denote the ensemble averaged expectation value. We introduce the dose dependence by describing two independent motor populations with a variable population fraction, taking the two populations to describe the subensemble of motors in the dark state (referred to here by the subscript "dark state") and the subensemble of motors in the lit state (referred here by the subscript "lit state"). We make the approximation that both populations have same spring constant κ, and we assume the two populations have the same motor kinetics, differing only in their stroke vectors yielding a distinct $\langle \xi_{dark\ state} \rangle$ and $\langle \xi_{lit\ state} \rangle$. This gives:

$$F = \kappa \left[\langle N_{dark\ state} \rangle \left(\langle \xi_{dark\ state} \rangle - \langle X \rangle \right) + \langle N_{lit\ state} \rangle \left(\langle \xi_{lit\ state} \rangle - \langle X \rangle \right) \right]$$

At steady state we assume that the track is moving at a constant velocity V, giving

$$\langle X \rangle = \langle Vt \rangle = V \langle t \rangle$$

where t is the amount of time that a motor has remained bound to the filament. For motor velocities in the range of micrometers per second, we neglect the hydrodynamic drag on the filament[1] so the net force is zero, and we can write

$$\langle N_{dark\ state}\rangle\ (\langle \xi_{dark\ state}\rangle - \ V\ \langle t\rangle\ ) = -\ (\langle N_{lit\ state}\ \rangle\ (\langle \xi_{lit\ state}\rangle - \ V\ \langle t\rangle\ )$$

Solving for the velocity V:

$$V = \frac{\langle \xi_{dark\ state}\rangle}{\langle t\rangle}\frac{\langle N_{dark\ state}\rangle}{\langle N_{dark\ state}\rangle + \ \langle N_{lit\ state}\rangle} \quad + \quad \frac{\langle \xi_{lit\ state}\rangle}{\langle t\rangle}\frac{\langle N_{lit\ state}\rangle}{\langle N_{dark\ state}\rangle + \ \langle N_{lit\ state}\rangle} \quad Eq.2$$

Now, recognizing

$$\varphi_{dark\ state} = \frac{\langle N_{dark\ state}\rangle}{\langle N_{dark\ state}\ \rangle + \ \langle N_{lit\ state}\rangle}\ , \varphi_{lit\ state} = \frac{\langle N_{lit\ state}\rangle}{\langle N_{dark\ state}\rangle + \ \langle N_{lit\ state}\rangle} \qquad Eq.3$$

as the fractional populations of motors in the dark and lit states, and

$$V_{dark\ state} = \frac{\langle \xi_{dark\ state}\ \rangle}{\langle t\rangle}\ , V_{lit\ state} = \frac{\langle \xi_{lit\ state}\rangle}{\langle t\rangle} \qquad Eq.4$$

as the velocities resulting from pure populations in the dark and lit state, respectively, we can express the dose-dependent velocity $V\ (I)$ as

$$V\ (I) = \ V_{dark\ state}\ \varphi_{dark\ state}(I) + \ V_{lit\ state}\ \varphi_{lit\ state}(I) \qquad Eq.5$$

Thus, under the assumptions of this very simplified model, the gliding filament velocity as a function of light dose (and as a function of time during transients after changing illumination conditions) can be written as a linear combination of velocities of the motors in the dark and lit states. Note that as described by Vilfan $\langle \xi \rangle$ and $\langle t \rangle$ may be related to the kinetics and lever arm displacements of transitions during a multistate motor cycle. In the simplest case where a power stroke of length d occurs rapidly after binding, followed by a single dominant dwell of characteristic time τ before detachment, we have $\langle \xi \rangle = d$ and $\langle t \rangle = \tau$ giving $V = \frac{d}{\tau}$.

Supplementary figures

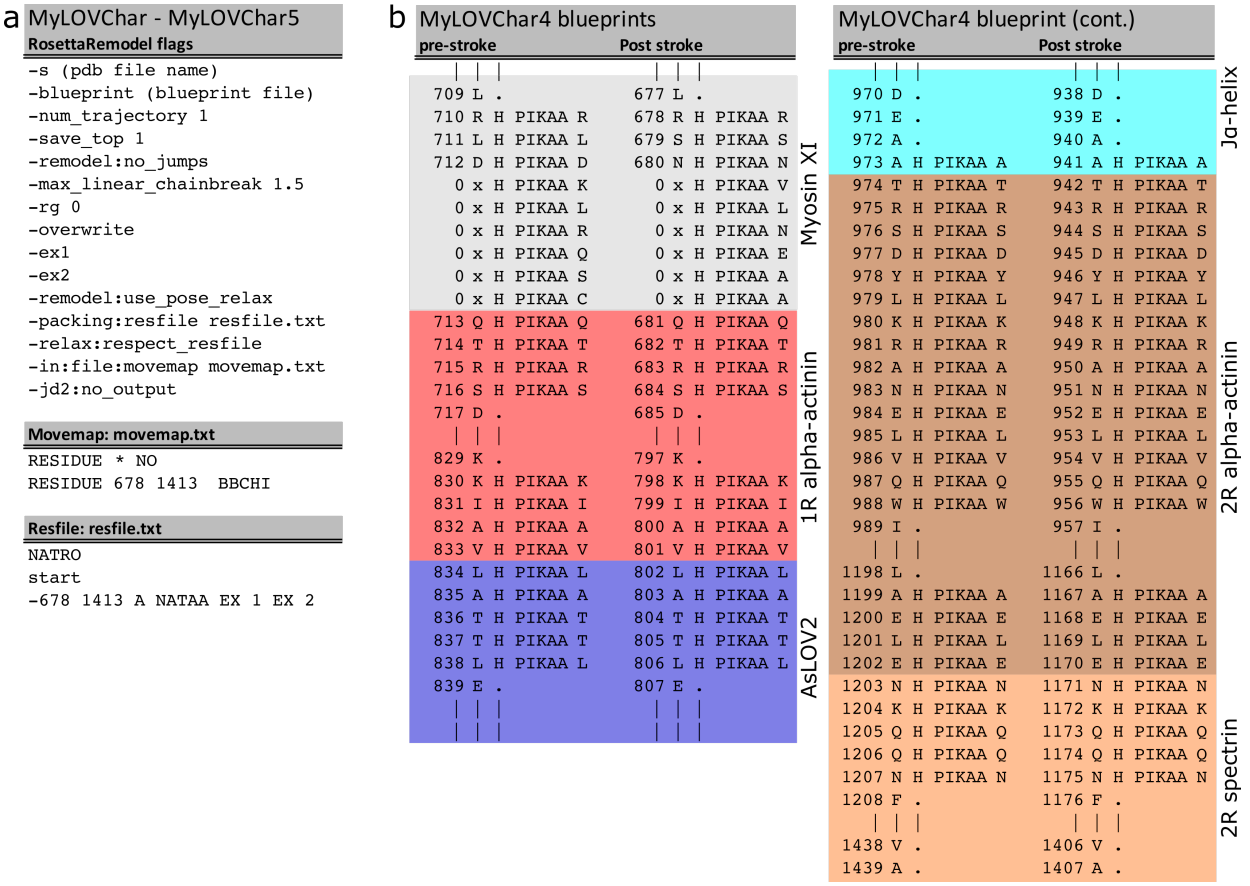

Supplementary Figure 1. RosettaRemodel parameters for models MyLOVChar-MyLOVChar5. a, RosettaRemodel parameters common to all models (MyLOVChar-MyLOVChar5 in both states). Shown movemap and resfile definitions apply to the post-stroke MyLOVChar4 model. Other models used analogous definitions, where atoms in the experimentally determined structures of the myosin catalytic domain were kept fixed, and all other residues were allowed to move. **b**, Blueprint file for pre-stroke and post-stroke models of MyLOVChar4. Other models in the series used an analogous setup. Sections of the models that were not remodeled by RosettaRemodel are omitted for brevity (indicated by rows with vertical dashes). Insertions of *de novo* built residues at the C-terminus of the myosin catalytic domain (after residue 680 in the Myosin XI numbering) were used since structural data was not available for this portion. The post-stroke

model used the native sequence of *Chara corallina* Myosin XI present in the experimental constructs. For the pre-stroke model the inserted residues were taken as the native Myosin Vc sequence, following the pre-stroke Myosin Vc structure used here as a model approximating the pre-stroke structure of the related Myosin XI.

Supplementary Figure 2. Molecular constructs. Junction and sequence information for molecular constructs generated in this study. Point mutations (in MyLOVChar and MyLOVChar2,

as in Nakamura et al.[3]) are indicated in bold. Residue insertions (in $CM11_{L2+4}CD746$) are indicated in bold and colored light blue. *: a sequence of TakaraBio I-dimerizer elements (not utilized in this study), a chemically inducible dimerization system. Here A/C heterodimerizer units are enchained, with two repeats of Heterodimerizer A, followed by Heterodimerizer C.

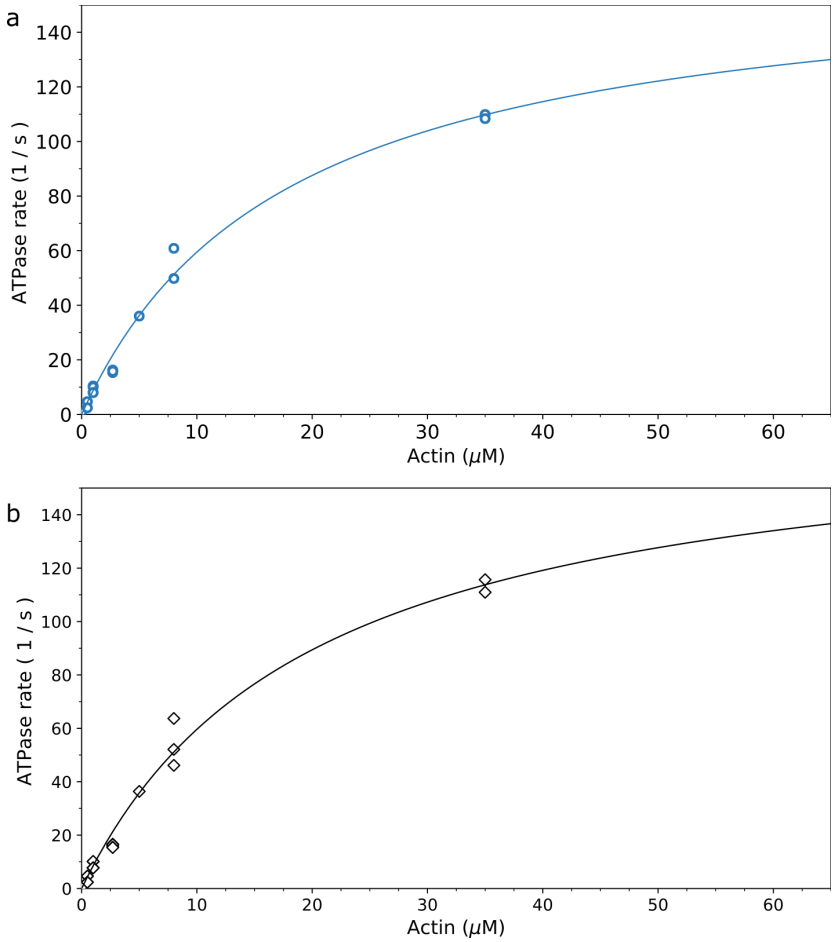

Supplementary Figure 3. ATPase activity of MyLOVChar4 in the presence and absence of blue light. Data are the results of the NADH-coupled assay shown in Fig. 1g in the main text, here showing datapoints for all individual measurements. **a**, data in presence of 10 mW/cm^2 blue light; **b**, data without blue light. Solid lines are reproduced from Fig. 1g, and are fits to a Michaelis-Menten expression, with k_{cat} = 180 s^{-1} and $K_{ATPase,\ actin}$ = 20 μM without blue light (**a**); k_{cat} = 160 s^{-1} and $K_{ATPase,\ actin}$ = 18 μM with blue light (**b**). The numbers of individual data points at each actin concentration are as follows: **a,** 0.5 μM: N=2, 1 μM: N=4, 2.7μM: N=4, 5 μM: N=1, 8μM: N=2, 35 μM: N=2; **b**, 0.5 μM: N=4, 1 μM: N=5, 2.7 μM: N=5, 5 μM: N=1, 8μM: N=3, 35 μM: N=2. All conditions with N>1 include measurements from two independent preparations of the assay.

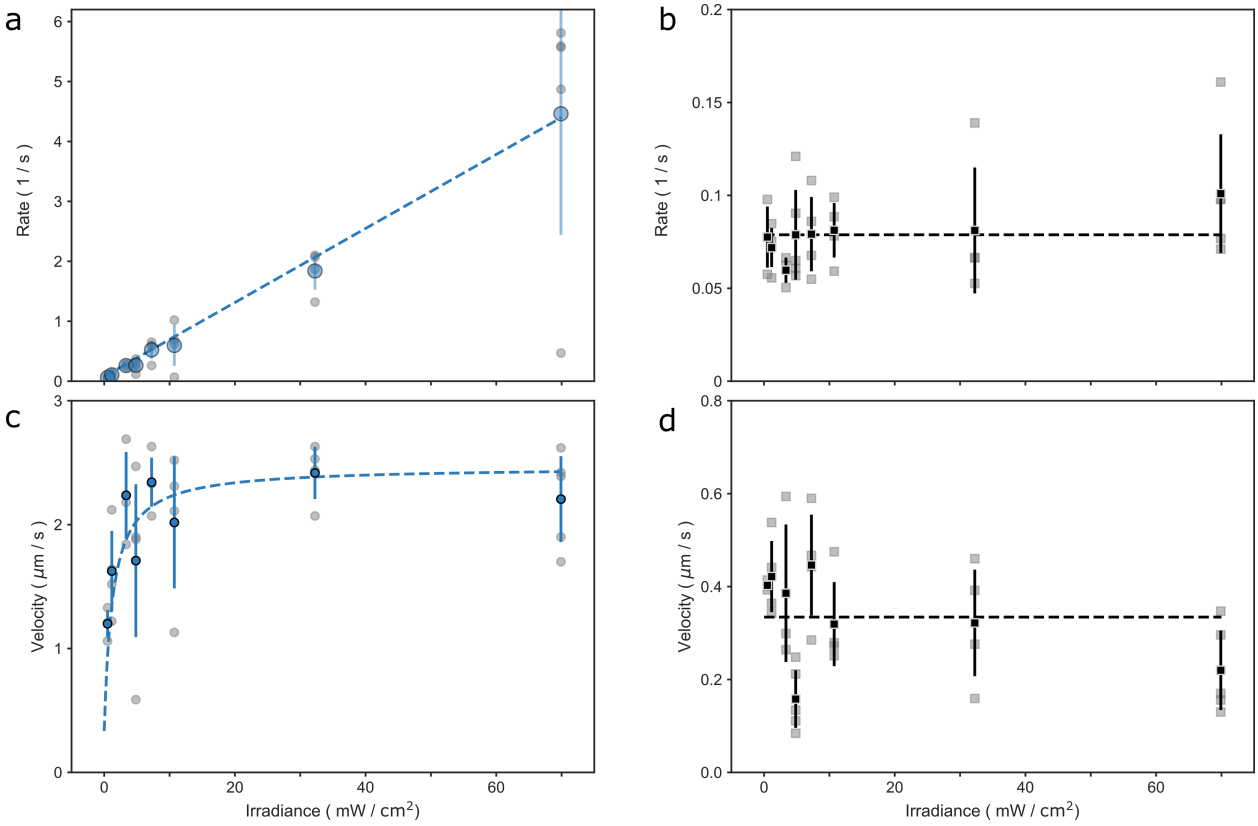

Supplementary Figure 4. Detail of characterization of MyLOVChar4 as function of blue light intensity. Averaged data and model fits are reproduced from Fig. 1h with the addition of dots (grey datapoints) representing individual replicates. **a**, k_{on}. **b**, k_{off}. **c**, $v_{\underline{lit}}$. **d**, v_{dark}. The number of independent assays at the blue light irradiance values in the dataset are as follows: 0.5 mW/cm^2: N=3, 1.2 mW/cm^2: N=4, 3.4 mW/cm^2: N=3, 4.8 mW/cm^2: N=5, 7.2 mW/cm^2: N=4, 10.7 mW/cm^2: N=4, 32.3 mW/cm^2: N=4, 70 mW/cm^2: N=5. Blue and black datapoints with error bars represent the mean ± standard deviation across replicates at each irradiance.

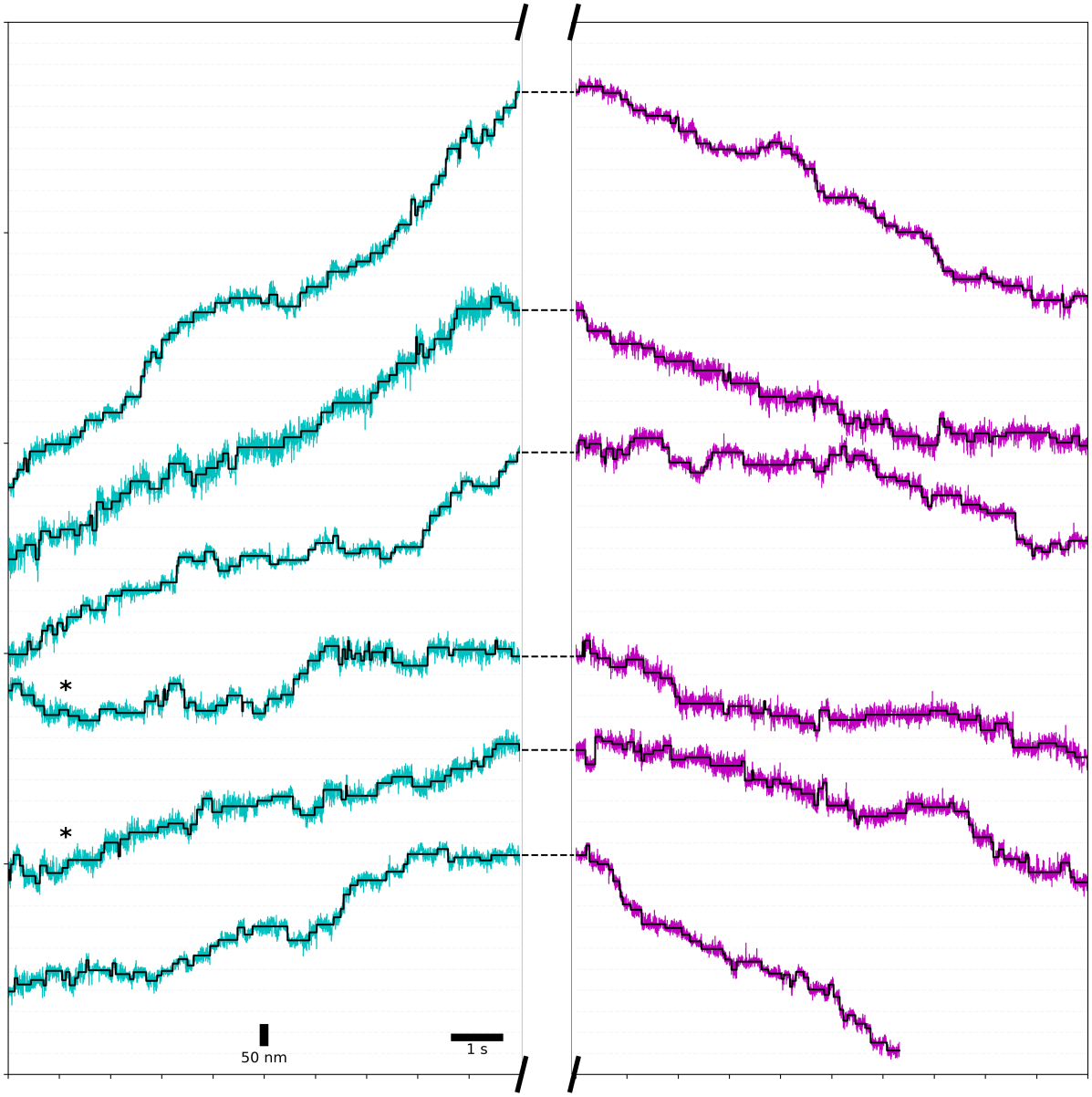

Supplementary Figure 5. Directional switching of gold nanoparticles. Gold nanoparticle motor tracking traces on MyLOVChar4$_{L2(+4)}$~1R~TET in presence and absence of blue light. We attribute each pair of stepping traces (connected with dashed lines) to a single nanoparticle that was tracked along one actin filament across two movies: one movie with blue light on (left) and one with blue light off (right). The broken time axis represents the time gap between the 2 movies

(~30 seconds). For the channels depicted here, there was a maximum of 0.07 moving nanoparticles per actin filament per 30 seconds of imaging, making it unlikely that the observed trajectories correspond to two distinct nanoparticles. Raw trajectories (cyan/magenta, acquired at 503 Hz) are shown together with fits (black) that are the result of an automated step-finding algorithm. Traces marked with an asterisk were acquired at 5 μM ATP, and the rest of the traces were acquired at 7 μM ATP.

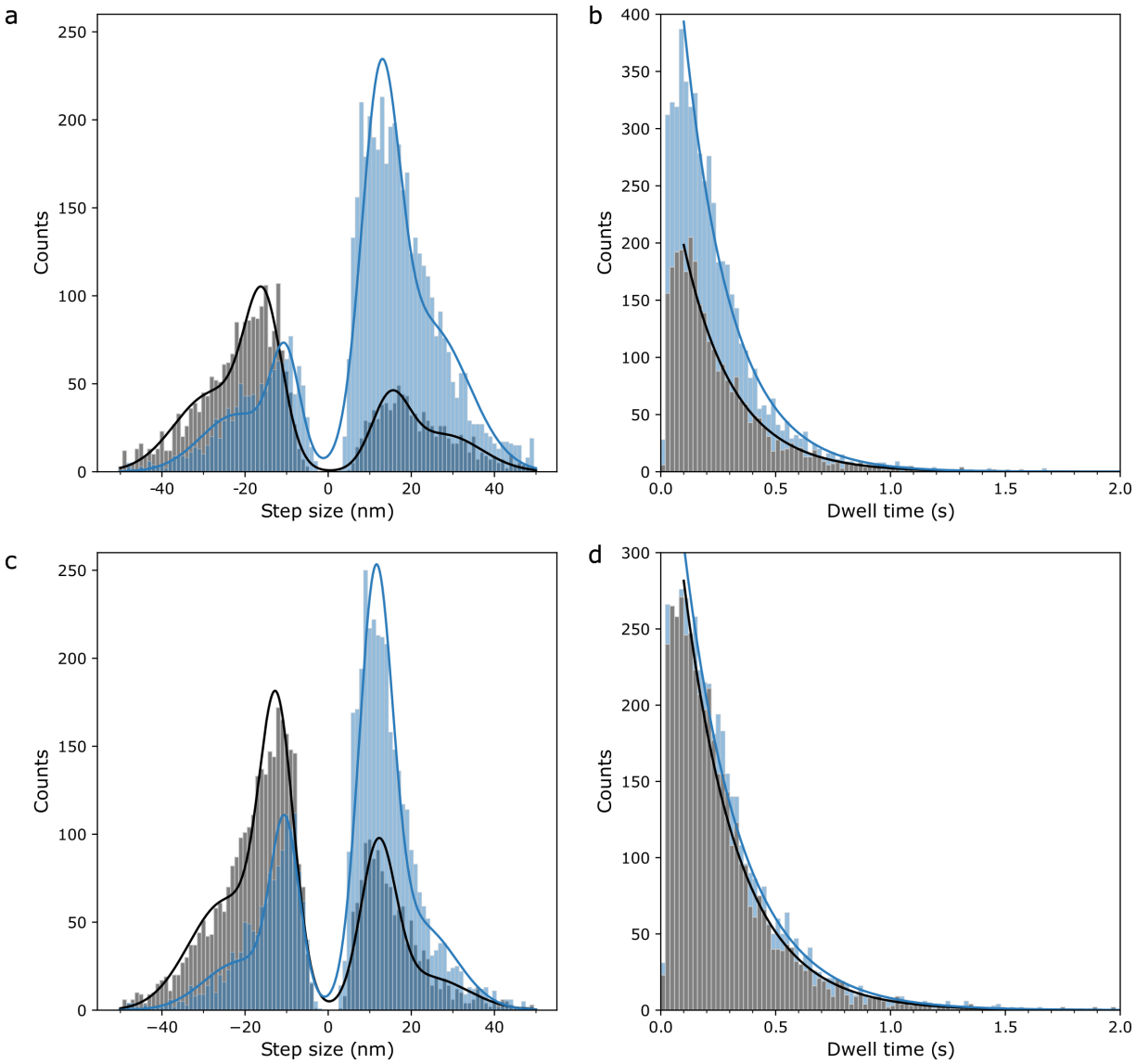

Supplementary Figure 6. Step size and dwell time histograms for MyLOVChar4L2(+4) ~1R~TET.

Step sizes (**l**eft) and dwell times (right) were calculated from gold nanoparticle tracking data at 7 μM ATP (top) and 5 μM ATP (bottom) using an automated step finding algorithm. Panel **c** reproduces the histogram data shown in Fig. 2b. Data collected with blue light off is are shown in gray with fits displayed as black lines, and data collected with blue light on are shown in blue with fits displayed as blue lines. The number of steps at 7 μM ATP are as follows. Blue off: N=2883; blue on: N=5387. The number of steps at 5 μM ATP are as follows. Blue off: N= 4364; blue on:

N=4809. The displayed axis range for dwell times excludes occasionally observed longer dwell times between 2-4 s (10 dwells for 5 μM ATP data with light, and 5 dwells for each of the other 3 conditions). Step size fits are Gaussian mixture models with the following peak locations. Blue off, 7 μM ATP: -28.1 ± 0.5 nm, -15.6 ± 0.3 nm, +15.0 ± 0.4 nm, +28.0 ± 0.6 nm. Blue on, 7 μM ATP: -21.8 ± 0.4 nm, -10.3 ± 0.4 nm, +12.5 ± 0.3 nm, +24.5 ± 0.3 nm. Blue off, 5 μM ATP: -24.7 ± 0.4 nm, -12.4 ± 0.3 nm, +12.1 ± 0.4 nm and +24.0 ± 0.9 nm. Blue on, 5 μM ATP: -20.9 ± 0.6 nm, -10.4 ± 0.3 nm, +11.4 ± 0.2 nm and 22.1 ± 0.4 nm. Dwell time fits are exponential distributions fit to data above a threshold of 0.1 second, with the following decay times. Blue off, 7 μM ATP: 0.217 ± 0.005 seconds. Blue on, 7 μM ATP: 0.204 ± 0.003 seconds. Blue off, 5 μM ATP: 0.235 ± 0.004 seconds. Blue on, 5 μM ATP: 0.246 ± 0.004 seconds. All fit values are reported as maximum likelihood estimates ± standard errors.

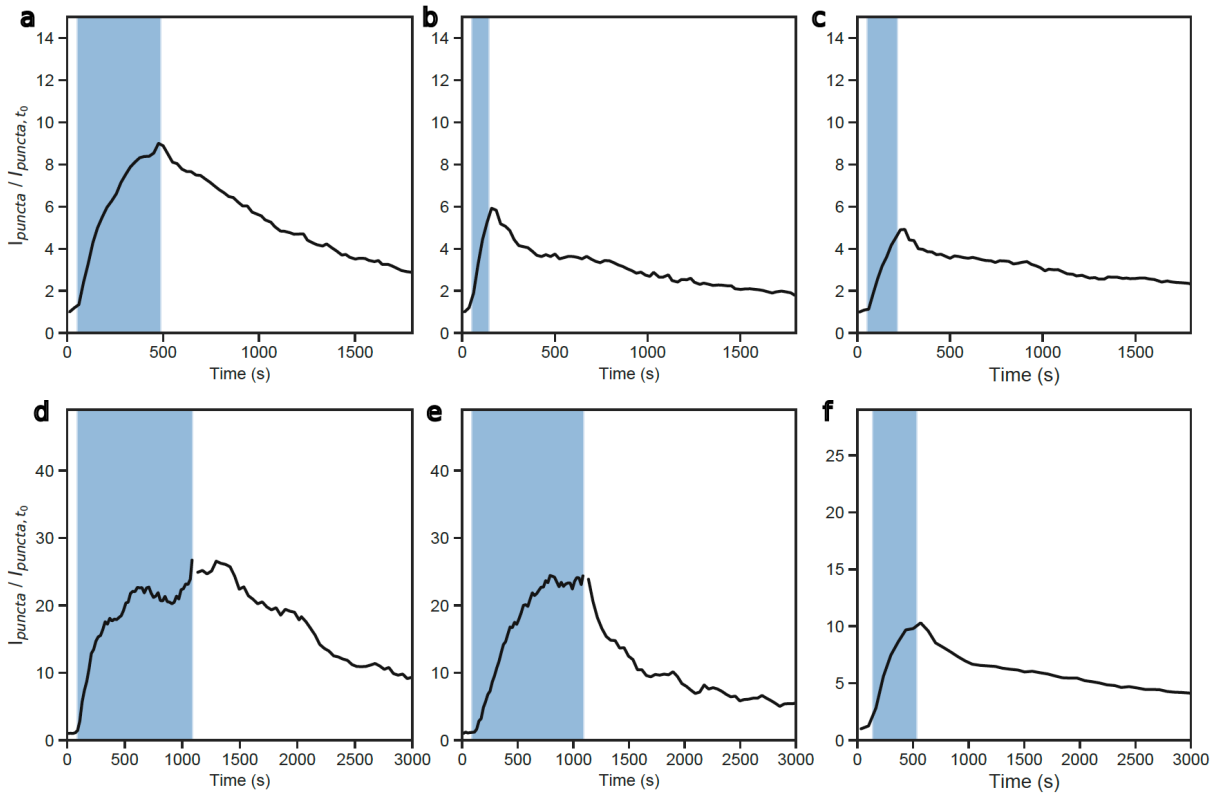

Supplementary Figure 7. Localization of motors in live cells in various single-pulse stimulation formats. Traces are from experiments performed on cells expressing MyLOVChar4~1R~TET-SNAP as in Fig. 3, with analysis carried out as in Fig. 3d. **a-c**, Traces with blue laser stimulation, co-scanning with the confocal image at 1% of nominal power. **d-f,** Traces with blue LED illumination. Blue light irradiances are 4.7 mW/cm^2 (**d**), 1.1 mW/cm^2 (**e**) and 2.0 mW/cm^2 (**f**).

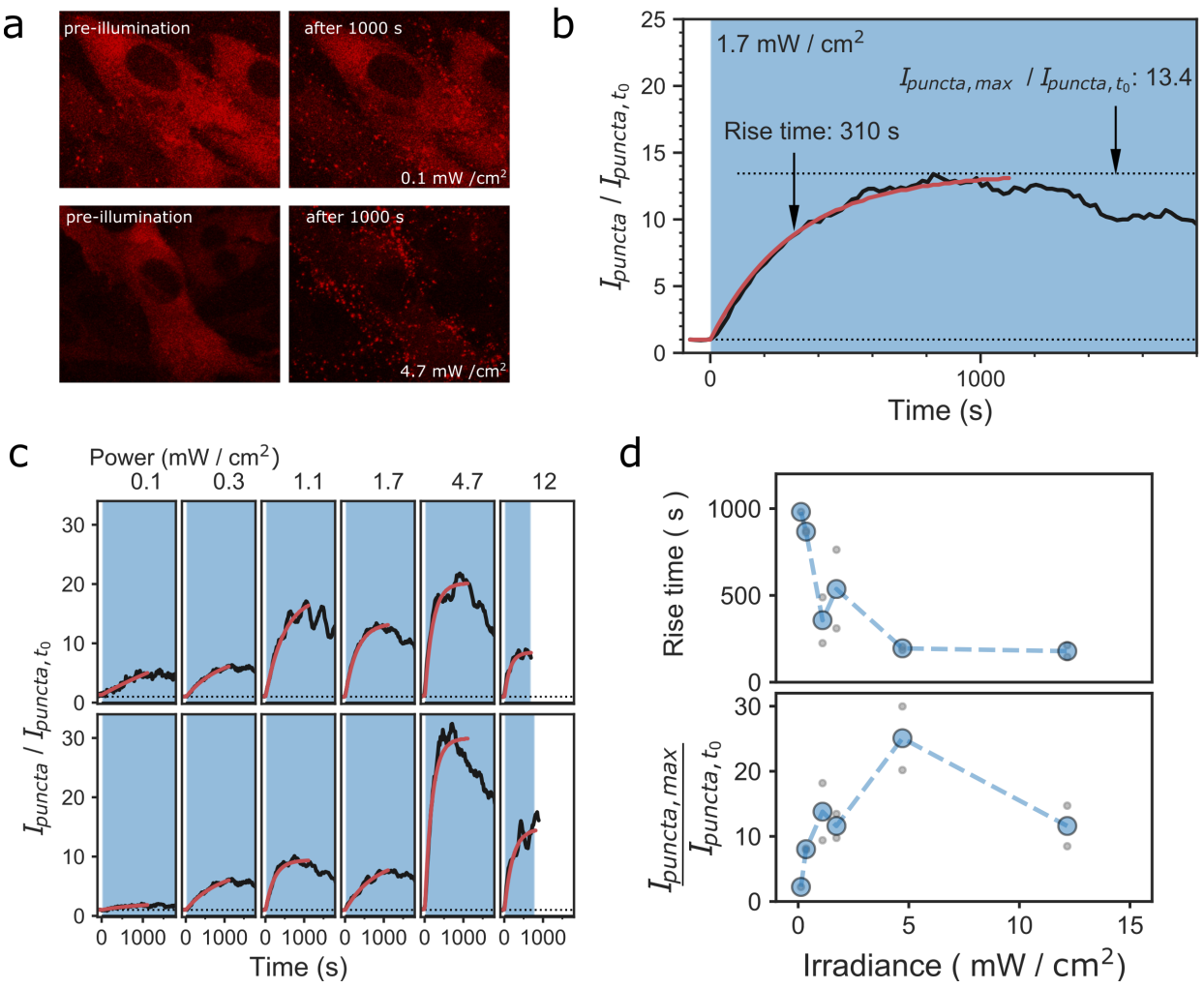

Supplementary Figure 8. Characterization of MyLOVChar4~1R~TET-SNAP in live cells as function of blue light irradiance. a, Cropped regions of imaged cultures of fibroblast cells expressing MyLOVChar4R1~1R~TET-SNAP-tag motors. Images, maximum intensity projection of the z-stack of confocal fluorescence images (excitation at 639 nm) before illumination (left columns) and after 1000 s of illumination with blue light (right columns). Top row, illumination with irradiance 0.1 mW/cm^2. Bottom row, illumination with irradiance 4.7 mW/cm^2. The full imaged areas contain between approximately 20 and 30 cells each. The images are representative of experiments replicated twice independently at each irradiance. **b**, Example trace following the intensity in puncta upon turning on blue light, at irradiance 1.7 mW/cm^2, after

normalization to the puncta intensity at the start of the image sequence. Red line is a single exponential fit to roughly approximate the transient, with annotated maximum and risetime used for analysis in panel d. **c**, Traces of intensity in puncta as in c, for increasing irradiance (columns 1-6), and two independent replicate experiments (top and bottom rows). **d**, Maximum puncta intensity and risetime as function of blue light irradiance. Blue points are the means of individual replicates (grey data points, N=2 independent replicate experiments).

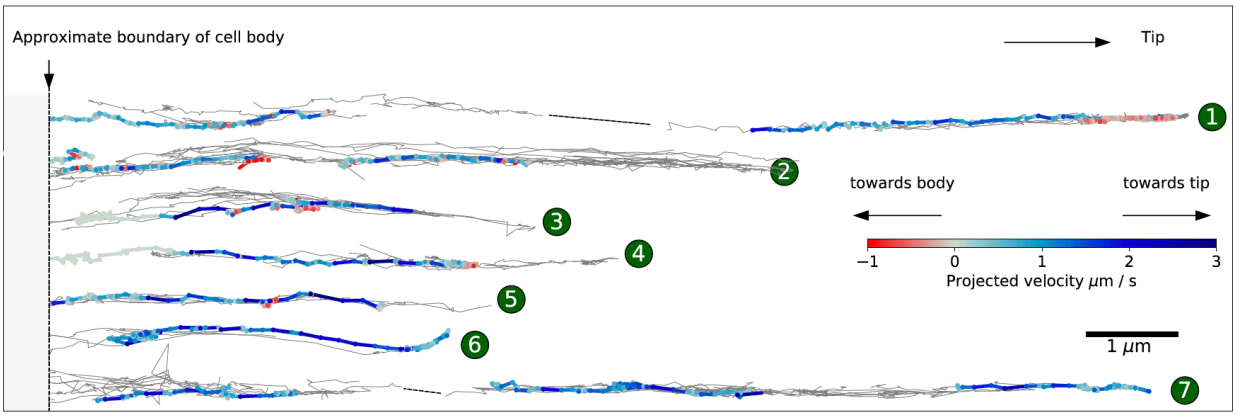

Supplementary Figure 9. Single-molecule tracking in cell protrusions. A series of tracks are shown for seven cell protrusions, labelled 1-7. The protrusions were defined manually by drawing spline interpolations (in ImageJ) at locations around the periphery of the cell where fluorescent spots were seen to closely follow the same trajectory, moving toward a bright spot. **Grey trajectories** show the full set of tracks associated with each protrusion. **Colored trajectories** are selected single trajectories, with color encoding the frame-to-frame velocity projected along the axis of the protrusion. For this display, each set of tracks was rotated and translated (maintaining spatial relationships between tracks) to follow horizontal lines with protrusion tips towards the right, and the approximate boundary of the cell body at a common x-coordinate. Black dotted lines are a guide to the eye to connect regions on protrusions 1 and 7 for which no tracks were detected.

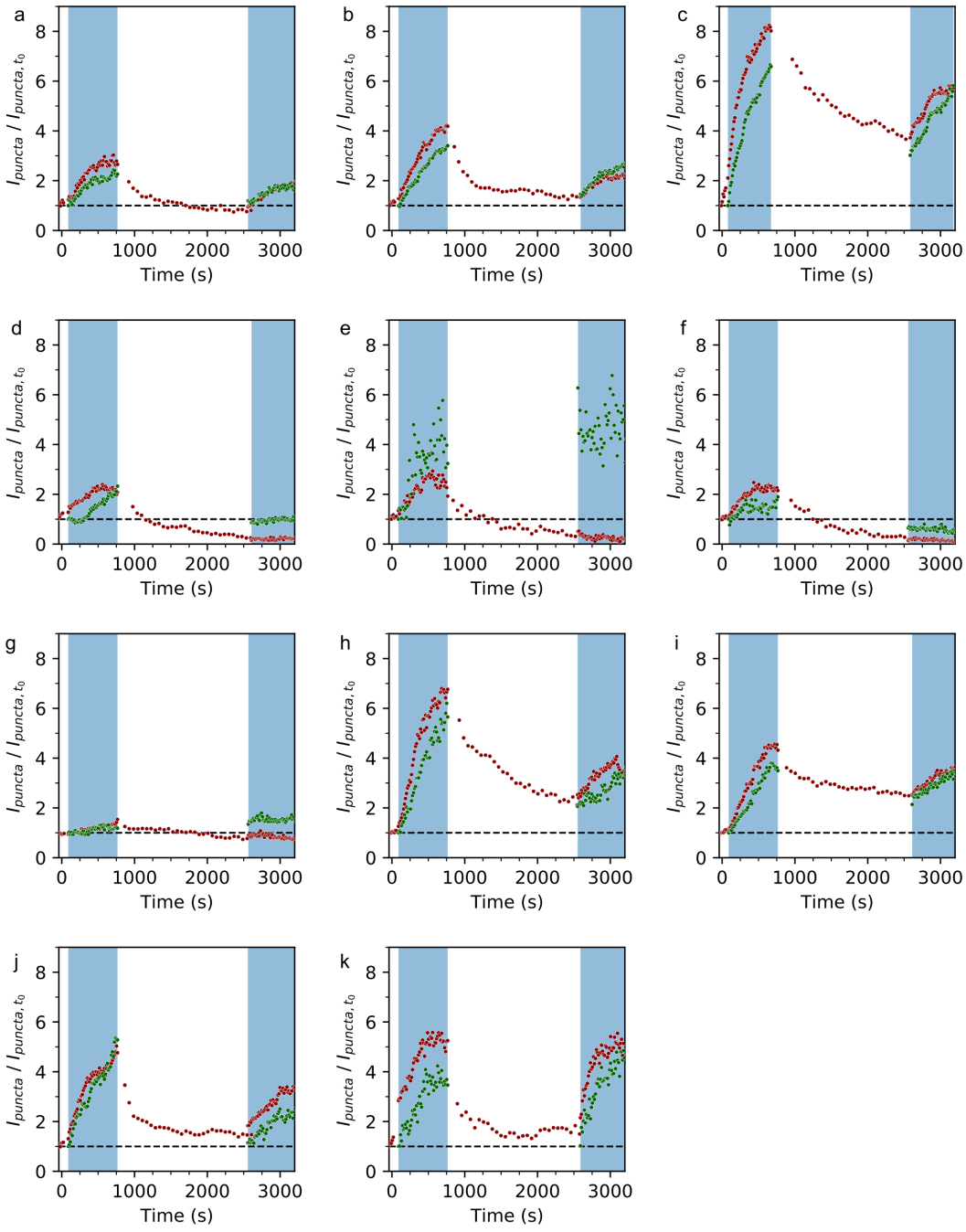

Supplementary Figure 10. Localization of motors and a FERM domain cargo in live cells. Data are from individual movie sequences on MCF10A cells expressing MyLOVChar4~1R~TET~DFHR and FERM~NB113~eGFP. The trace in panel **c** corresponds to the cell shown in Fig. 5b. Sequences in panel **g** and **i** correspond to image crops containing two cells; all other sequences were obtained on image crops around a single cell. All of these data except for panel **c** (which was

acquired with a 12.5% reduced frame rate and illumination period during each illumination period) were used to compute the averaged response shown in Fig. 5c. Most individual sequences display the characteristic response pattern represented in the average, but there is some variability owing to experimental heterogeneity and/or limitations of the simple analysis protocol (see Methods).

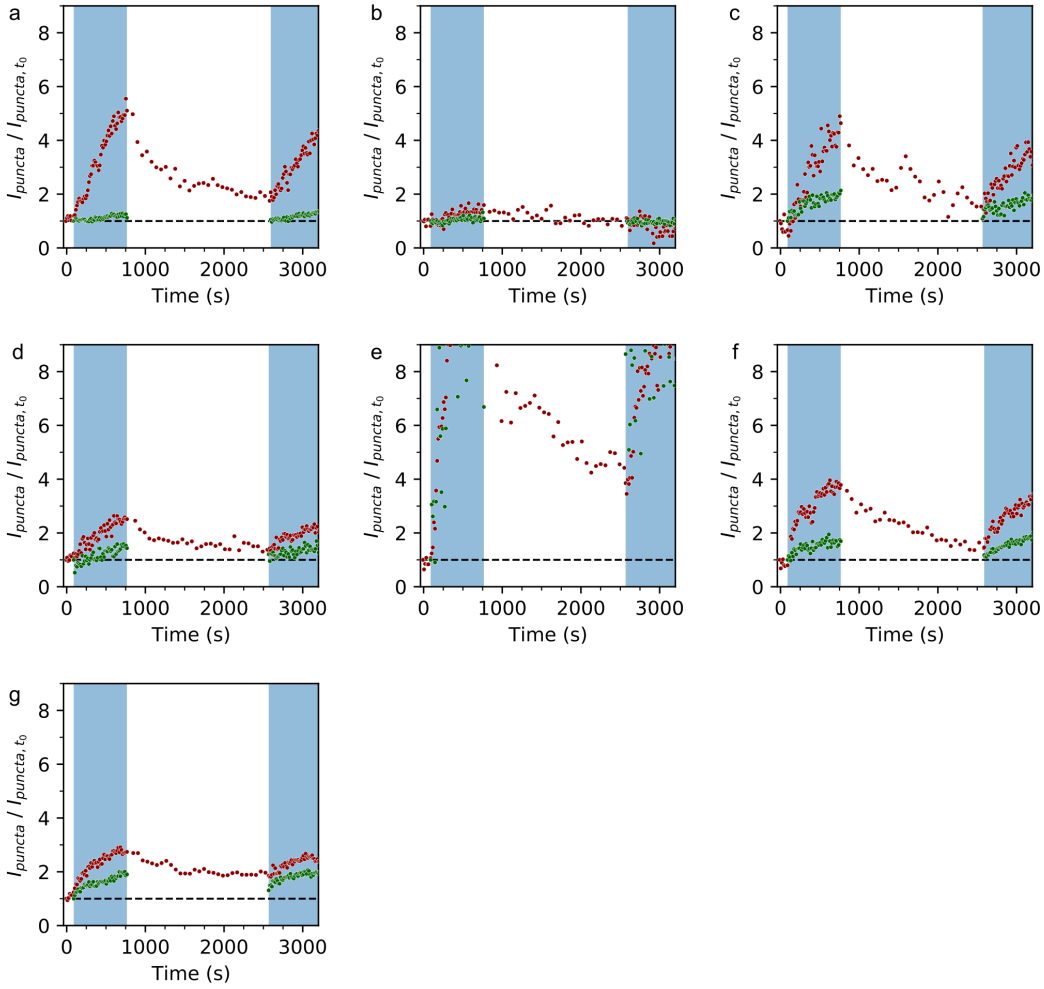

Supplementary Figure 11. Localization of motors and an integrin β3 cargo in live cells. Data are from individual movie sequences on MCF10A cells expressing MyLOVChar4~1R~TET~DFHR and integrin β3~NB113~eGFP, with most sequences displaying the characteristic response pattern, but some variability as in Supplementary Figure 10. The trace in panel **g** corresponds to the image shown in Fig 5d. The sequence in panel **a** was obtained from a movie crop containing two cells; each of the other sequences were cropped around one cell. All of these data were used to compute the averaged response shown in Fig. 5e.

Supplementary tables

	Myosin 11 bound F- actin (EMDB-22808) (PDB 7KCH)
Data collection and processing	
Magnification	105,000
Voltage (kV)	300
Electron exposure (e–/Å^2)	67.12
Defocus range (μm)	-1.0 to -4.0
Pixel size (Å)	1.1
Symmetry imposed	C1
Initial particle images (no.)	72,336
Final particle images (no.)	45,779
Map resolution (Å)	4.33
FSC threshold	0.143
Map resolution range (Å)	4.33 to 8.5
Refinement	
Initial model used (PDB code)	6BNO
Model resolution (Å)	4.3
FSC threshold	0.5
Model resolution range (Å)	256.0 to 4.3
Map sharpening *B* factor (Å^2)	-104
Model composition	3 actin protomers, 1 myosin 11
Non-hydrogen atoms	12,248
Protein residues	1,805
Ligands	3 Mg.ADP
B factors (Å^2)	
Protein	106.43
Ligand	87.36
R.m.s. deviations	
Bond lengths (Å)	0.011
Bond angles (°)	1.068
Validation	
MolProbity score	2.85
Clashscore	19.16
Poor rotamers (%)	4.72
Ramachandran plot	
Favored (%)	89.5
Allowed (%)	10.5
Disallowed (%)	0.00

Supplementary Table 1. Cryo-EM data collection, refinement and validation statistics.

Reference	Imaging mode (Blue light stimulus mode)	Motor construct	Fluorescent label / optical readout	Exc. λ(nm)	Blue Exc. λ(nm)
Fig 1c-f, h	TIRF (LED CW)	MyLOVChar MyLOVChar2 MyLOVChar3 MyLOVChar4 MyLOVChar5	TMR phalloidin, Cy-5	532, 633	470
Fig 1g	Spectrophotometer, Xe lamp (LED CW)	MyLOVChar4	NADH*	340	470
Fig 2a	TIRF (LED CW)	MyLOVChar4 ~ 1R ~ TET	Halotag Alexa 660	633	470
Fig 2b	TIR scattering (LED CW)	MyLOVChar4$_{L2(+4)}$ ~ 1R ~ TET	50 nm gold nanoparticle	532	470
Fig 3c	Laser scanning confocal (Laser scanning confocal)	MyLOVChar4 ~ 1R ~ TET ~ SNAP	SNAP-Cell® 647-SiR	639	488
Fig 3d	Laser scanning confocal (Laser scanning confocal)	MyLOVChar4 ~ 1R ~ TET ~ SNAP	SNAP-Cell® 647-SiR	639	488
Fig 3e	Laser scanning confocal (LED CW)	MyLOVChar4 ~ 1R ~ TET ~ SNAP	SNAP-Cell® 647-SiR	639	470
Fig 3f	Laser scanning confocal (LED 500Hz PW modulation)	MyLOVChar4 ~ 1R ~ TET ~ SNAP	SNAP-Cell® 647-SiR	639	470
Fig. 3h	Wide-field epi, Xe lamp (LED CW)	MyLOVChar4 ~ 1R ~ TET ~ mRuby3	mRuby3	568 ± 10	470
Fig 4c-h	HILO (HILO)	MyLOVChar4 ~1R~ TET ~ ArrayG$_{16X}$	mwtGFP	488	488
Fig 5c-d	Laser scanning confocal (Laser scanning confocal)	MyLOVChar4~1R~TET ~ SNAP ~ DHFR, FERM ~ NB113 ~ eGFP,	mwtGFP	488	488
Fig 5d-e	Laser scanning confocal (Laser scanning confocal)	MyLOVChar4~1R~TET-SNAP-DHFR, IntegrinBeta3 ~ NB113 ~ eGFP,	mwtGFP	488	488
Extended Data Fig. 3	TIRF (LED CW)	MyLOVChar4	TMR phalloidin, Cy-5	532, 633	470
Extended Data Fig. 4	Fluorimeter, Xe lamp (LED CW)	SNAP ~ 1R-LOV-1R ~ HT	SNAP-Cell® 647-SiR Halotag TMR	532 ± 5	470
Extended Data Fig. 5	Wide-field epi, Xe lamp (LED CW)	MyLOVChar4 ~ 1R ~ TET ~ mRuby3	mRuby3	568 ± 10	470
Extended Data Fig 6	Laser scanning confocal (Laser scanning confocal)	MyLOVChar4 ~ 1R ~ TET ~ SNAP ~ tdPCP, PP7~BetaACTIN~MS2$_{24X,}$ MCP ~ mNeon	mNeon	488	488
Supp. Fig. 3	Spectrophotometer, Xe lamp (LED CW)	MyLOVChar4	NADH*	340	470
Supp. Fig. 4	TIRF (LED CW)	MyLOVChar4	TMR phalloidin, Cy-5	532, 633	470
Supp. Fig. 5,6	TIR scattering (LED CW)	MyLOVChar4$_{L2(+4)}$ ~ 1R ~ TET	50 nm gold nanoparticle	532	470
Supp. Fig. 7 a-c	Laser scanning confocal (Laser scanning confocal)	MyLOVChar4 ~ 1R ~ TET ~ SNAP	SNAP-Cell® 647-SiR	639	470
Supp. Fig. 7 d-f	Laser scanning confocal (LED CW)	MyLOVChar4 ~ 1R ~ TET ~ SNAP	SNAP-Cell® 647-SiR	639	470
Supp. Fig. 8	Laser scanning confocal (LED 500Hz PW modulation)	MyLOVChar4 ~ 1R ~ TET ~ SNAP	SNAP-Cell® 647-SiR	639	470
Supp. Fig. 9	HILO (HILO)	MyLOVChar4 ~ 1R ~ TET ~ ArrayG$_{16X}$	mwtGFP	488	488

*NADH: nicotinamide adenine dinucleotide (reduced)

Supplementary Table 2. Overview of blue light stimulation conditions.

References

1 Vilfan, A. Ensemble velocity of non-processive molecular motors with multiple chemical states. *Interface Focus* **4**, 20140032 (2014).

2 Leibler, S. & Huse, D. A. Porters versus rowers: a unified stochastic model of motor proteins. *Journal of Cell Biology* **121**, 1357-1368 (1993).

3 Nakamura, M. *et al.* Remote control of myosin and kinesin motors using light-activated gearshifting. *Nat Nanotechnol* **9**, 693-697 (2014).